***New Phytologist* Supporting Information**

Article title: **A host target of a bacterial cysteine protease virulence effector plays a key role in convergent evolution of plant innate immune system receptors**

Authors: Maxim Prokchorchik[1,2], Sera Choi[1], Eui-Hwan Chung[4,5], Kyungho Won[6], Jeffery L. Dangl[4,5] and Kee Hoon Sohn[1,3]

Article acceptance date: 17 September 2019

The following Supporting Information is available for this article:

Fig. S1 Phylogenetic analysis of the selected CNLs from multiple plant species.

Fig. S2 MdRIN4-2 and RIN4 homologs from *Pyrus* species can activate MR5 upon AvrRpt2-directed cleavage.

Fig. S3 RIN4 homologs from *N. benthamiana* cannot suppress RPS2 auto-activity or activate MR5 when co-expressed with EaAvrRpt2.

Fig. S4 Phylogenetic tree of RIN4 homologs from diverse plant species.

Fig. S5 F179A substitution of MdRIN4 abolish AvrRpt2-triggered and MR5-dependent induction of ion leakage.

Fig. S6 Reciprocal mutations at D/N or F/Y amino acid residues dramatically alter chimeric RIN4 ACP3 function.

Fig. S7 MdRIN4$^{D186N/F193Y}$ suppresses RPS2 auto-activity when co-expressed with AvrRpt2.

Fig. S8 Full-length RIN4 variants with mutations in polymorphic residues accumulate to higher levels and can be eliminated by AvrRpt2 when expressed *in planta*.

Fig. S9 The palmitoylation sequence motif is required for function of RIN4 full-length and ACP3 variants carrying reciprocal mutations at D/N or F/Y amino acid residues.

Fig. S10 MdRIN4$^{D186N/F193Y}$ ACP3 variant can suppress RPM1 and RPS2 mediated autoimmunity.

Fig. S11 RIN4 transgene expression in Arabidopsis transgenic lines.

Table S1 Primers used in this study

Table S2 Table of approximate molecular weights of protein products and their fragments used in this study

Methods S1 RIN4 homolog and CNL phylogenetic analysis

Methods S2 Quantitative RT-PCR

Fig. S1 Phylogenetic analysis of the selected CNLs from multiple plant species. The CC and NB domain protein sequences of CNLs were aligned with ClustalW and a Neighbor-Joining tree was inferred from the alignment. Node labels represent bootstrap support values. RPM1, RPS2 and MR5 are highlighted with blue boxes.

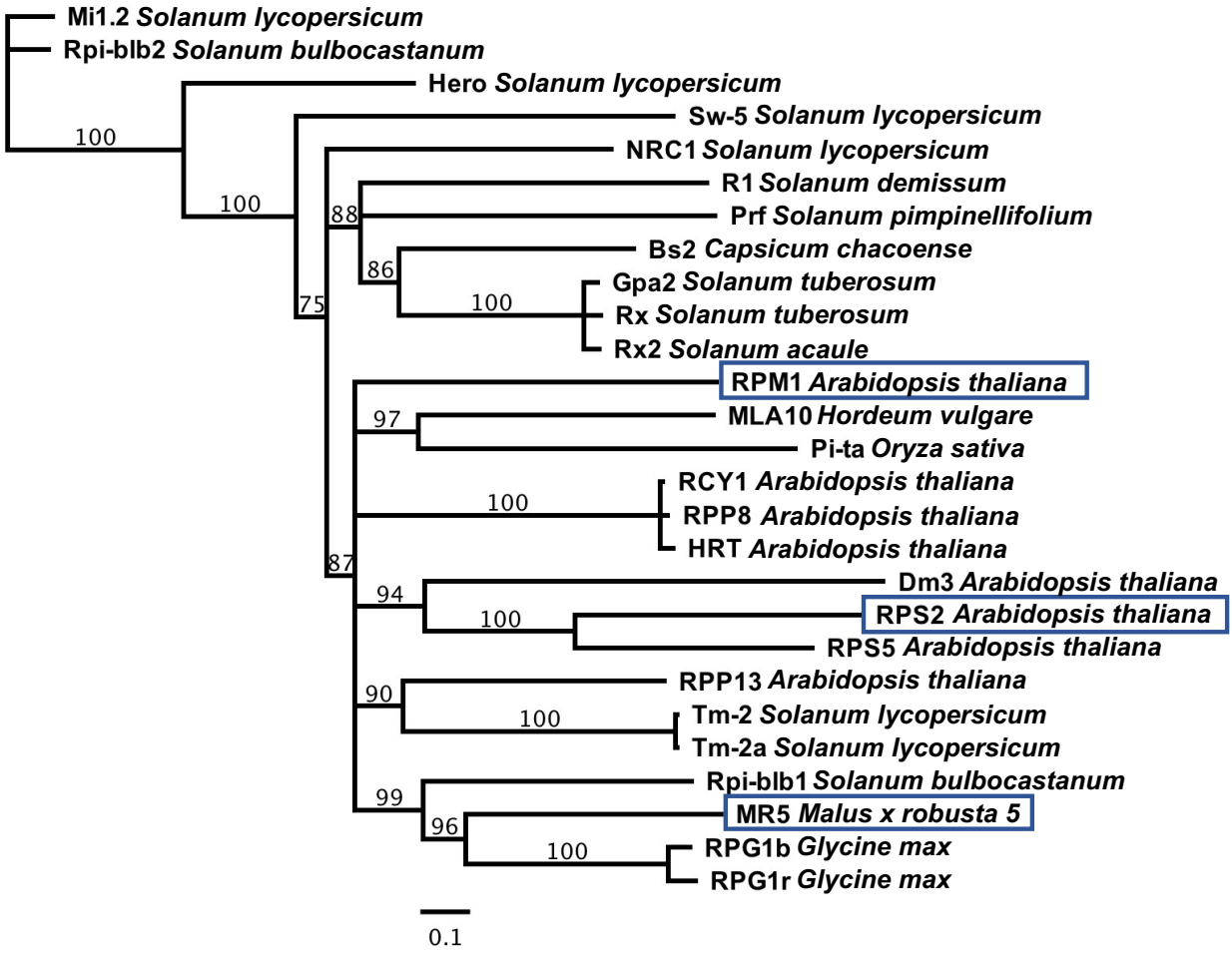

Fig. S2 MdRIN4-2 and RIN4 homologs from *Pyrus* species can activate MR5 upon AvrRpt2-directed cleavage. (a) and (b) Proteins were expressed in *N. benthamiana* leaves by agroinfiltration, using the following OD_{600} for Agrobacterium strains carrying the following constructs: MdRIN4-2 and other RIN4 homologs or MR5 – 0.4, AvrRpt2 variants – 0.05. PpRIN4 is a RIN4 homolog from *Pyrus pyrifolia* and PuRIN4 is a homolog from *Pyrus ussuriensis*. PCD symptoms were photographed at 3 dpi. Yellow asterisks indicate agroinfiltrated leaf area showing PCD.

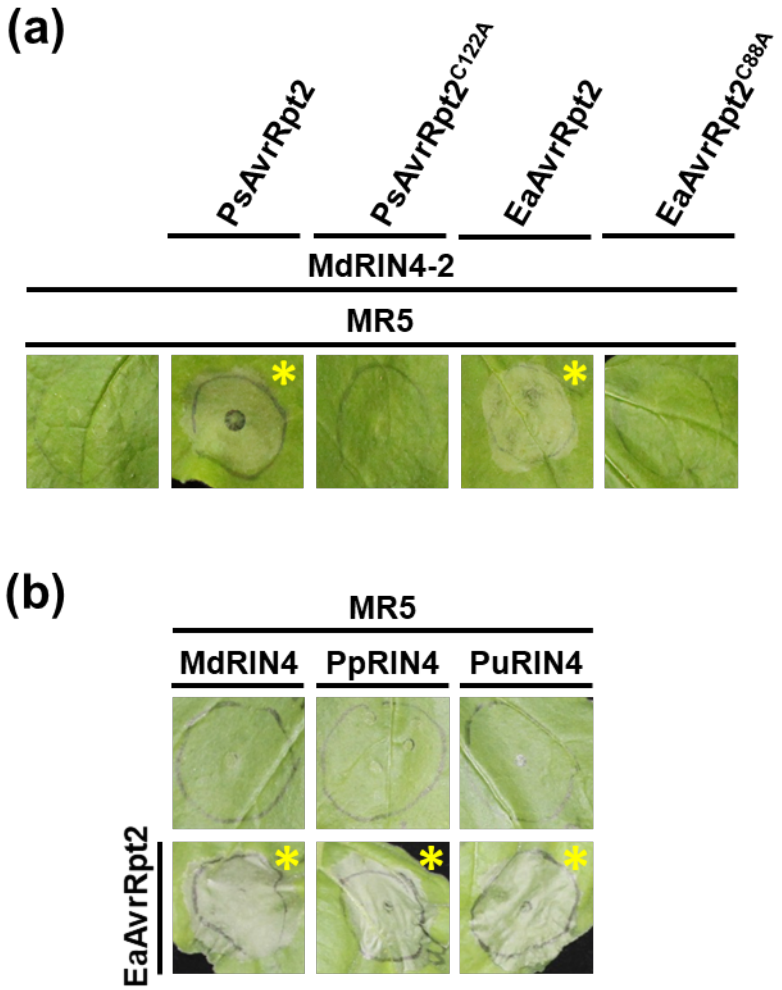

Fig. S3 RIN4 homologs from *N. benthamiana* cannot suppress RPS2 auto-activity or activate MR5 when co-expressed with EaAvrRpt2.

(a) Agroinfiltration was carried out as described in Fig. S2. PCD symptoms were photographed at 3 dpi. Yellow asterisks indicate agroinfiltrated leaf area showing PCD.

(b) *In planta* processing of NbRIN4 variants by EaAvrRpt2. Protein bands corresponding to the unprocessed and processed AvrRpt2 are marked with single and double asterisk, respectively. Agroinfiltration was carried out as described in (a). Leaf samples were collected at 2 dpi and protein extracts were probed with anti-Myc or anti-HA antibodies. Ponceau staining the RuBisCO large subunit is provided to show equal protein loading. Accession numbers for *NbRIN4* genes are NbRIN4-1 (Genbank: KX272617.1), NbRIN4-2 (Solgenomics predicted gene ID: Niben101Scf08799g00001) and NbRIN4-3 (Solgenomics predicted gene ID: Niben101Scf03488g06005.1).

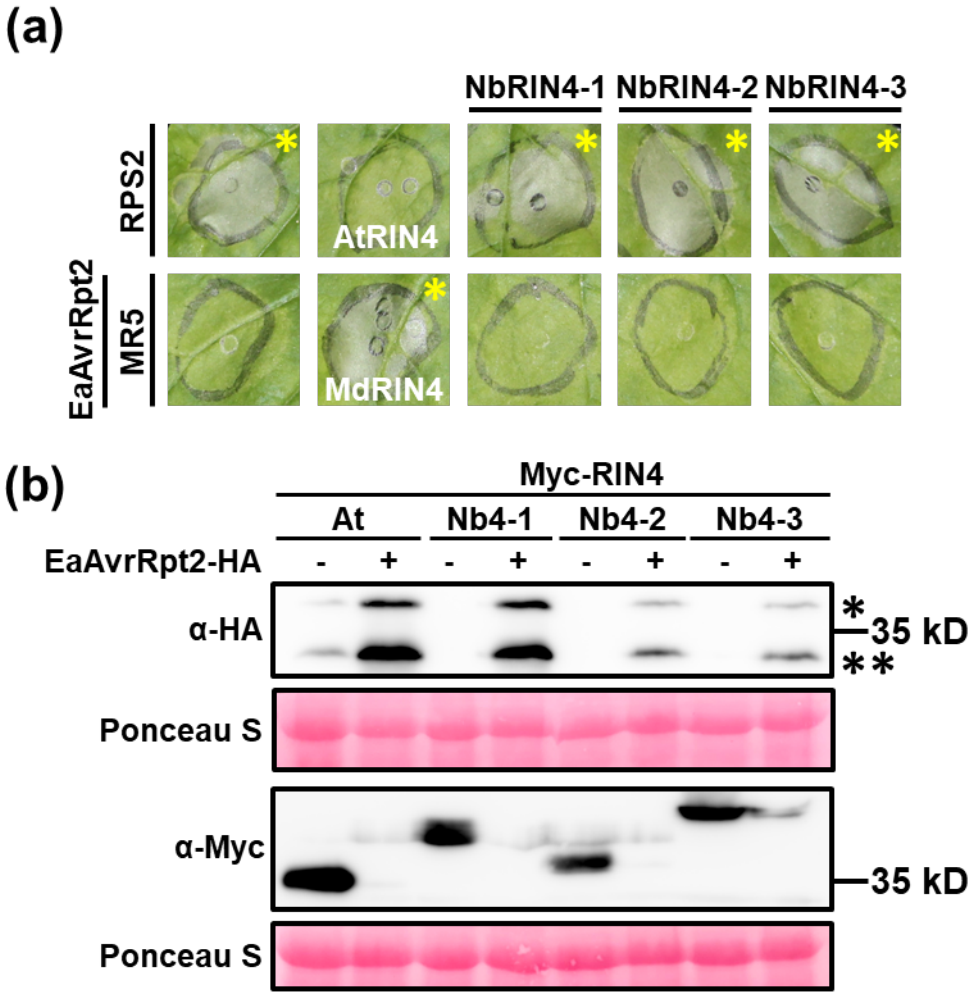

Fig. S4 Phylogenetic tree of RIN4 homologs from diverse plant species. Protein sequences of RIN4 homologs were aligned with ClustalW and a Neighbor-Joining tree was inferred from the alignment. Node labels represent bootstrap support values. AtRIN4, GmRIN4 and MdRIN4 homologs are highlighted with red font.

Fig. S5 F179A substitution of MdRIN4 abolish AvrRpt2-triggered and MR5-dependent induction of ion leakage. MR5 (OD_{600}=0.4), RIN4 variants (OD_{600}=0.4) and AvrRpt2 variants (OD_{600}=0.05) were co-expressed in *N. benthamiana* leaves by agroinfiltration. Each bar represents mean of 4 electrolyte leakage measurements. Error bars represent S.E.M. Statistical significance was assessed by one-way ANOVA test followed by Tukey-Kramer HSD analysis. Bars labeled with identical letter indicate that there is no significant statistical difference (*P*-value < 0.05). The experiment was conducted twice with similar results.

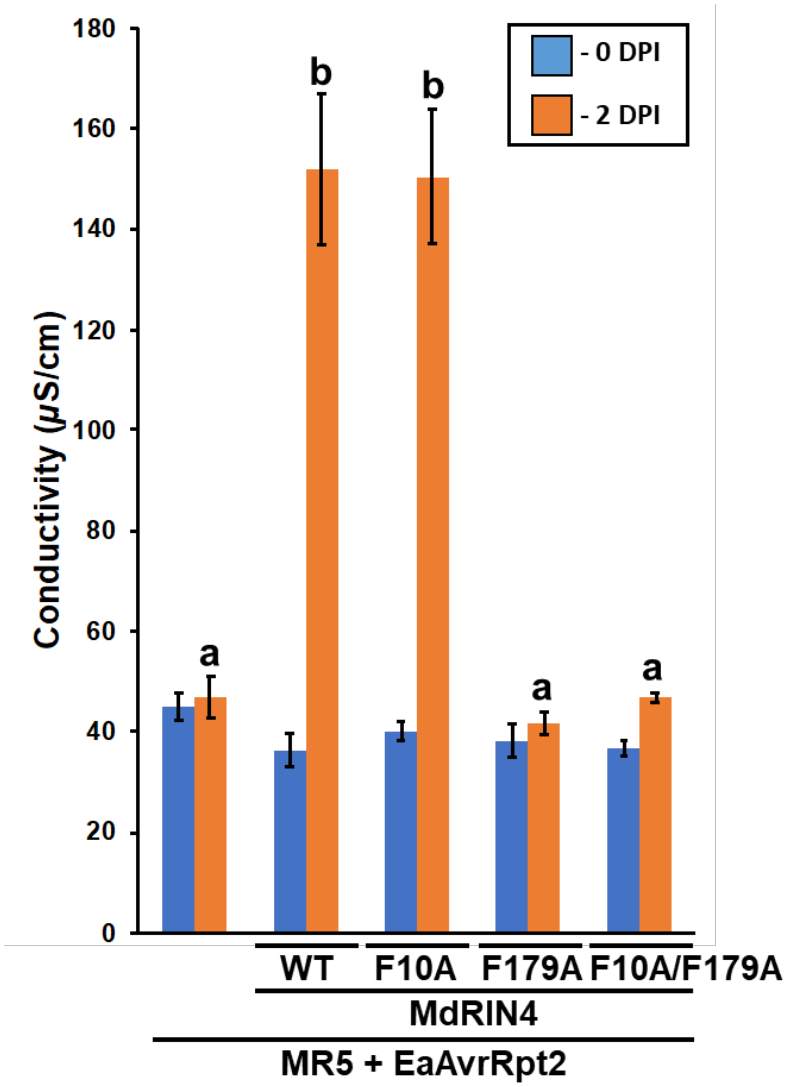

Fig. S6 Reciprocal mutations at D/N or F/Y amino acid residues dramatically alter chimeric RIN4 ACP3 function. The polymorphic amino acid residues in the C-NOI fraction of RIN4 ACP3 chimeric proteins where mutated to the ones from the other RIN4 homolog using site-directed mutagenesis. Resulting constructs were expressed via agroinfiltration in *N. benthamiana* leaves. Strains carrying constructs coding for RIN4 ACP3 chimeras with or without mutations were infiltrated at OD_{600} – 0.4, MR5 – 0.4. PCD symptoms were photographed at 3 dpi. Yellow asterisks indicate agroinfiltrated leaf area showing PCD.

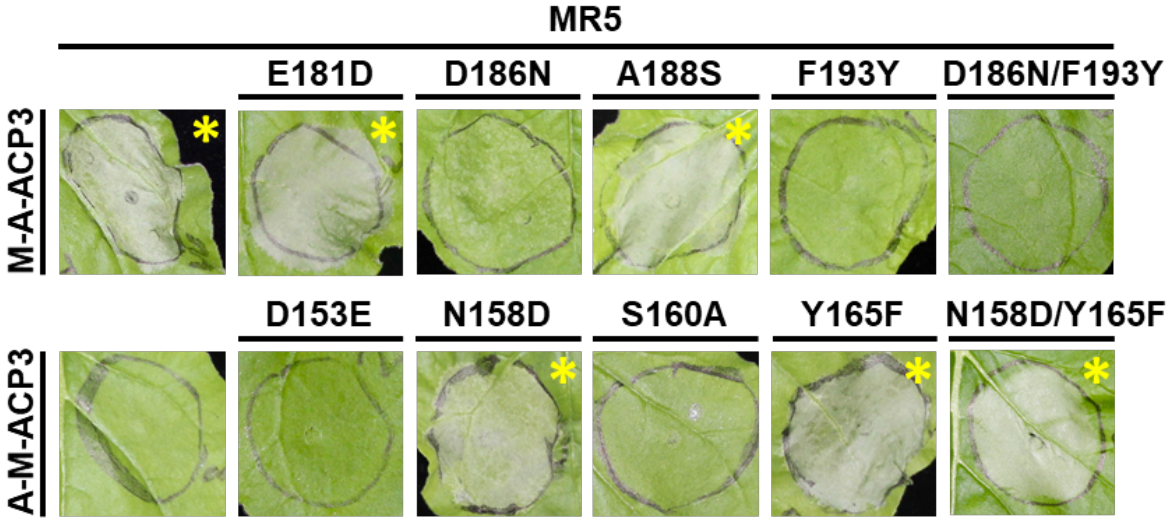

Fig. S7 MdRIN4$^{D186N/F193Y}$ suppresses RPS2 auto-activity when co-expressed with AvrRpt2. RPS2 (OD_{600}=0.1), RIN4 variants (OD_{600}=0.4) and AvrRpt2 variants (OD_{600}=0.05) were co-expressed in *N. benthamiana* leaves by agroinfiltration. C88A stands for EaAvrRpt2^{C88A} and N+Y for MdRIN4$^{D186N/F193Y}$. Graph represents electrolyte leakage levels measured in the infected leaf samples. Each bar represents mean of 8 electrolyte leakage measurements. Error bars represent S.E.M. Statistical significance was assessed by one-way ANOVA test followed by Tukey-Kramer HSD analysis. Bars labeled with identical letter indicate that there is no significant statistical difference (*P*-value < 0.05). The experiment was conducted three times with similar results.

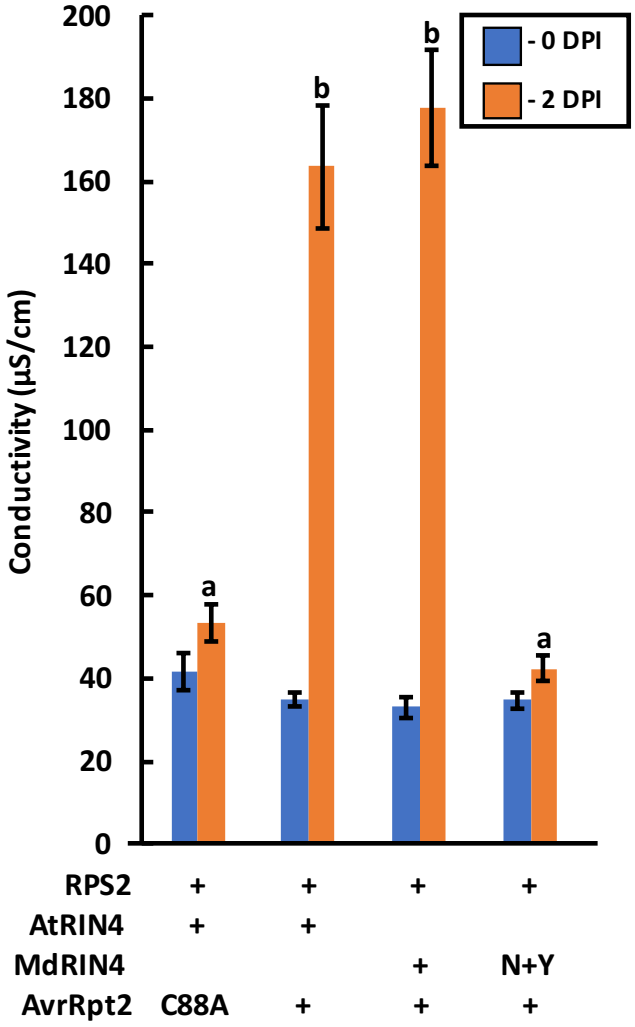

Fig. S8 Full-length RIN4 variants with mutations in polymorphic residues accumulate to higher levels and can be eliminated by AvrRpt2 when expressed *in planta*. Protein bands corresponding to the unprocessed and processed AvrRpt2 are marked with single and double asterisks, respectively. Agrobacterium strains carrying constructs coding for RIN4 full-length variants with or without mutations and EaAvrRpt2 were infiltrated into *N. benthamiana* leaves at OD_{600}=0.4 and OD_{600}=0.1, respectively. Leaf samples were collected at 2 dpi and protein extracts probed with anti-Myc or anti-HA antibodies. Ponceau staining the RuBisCO large subunit is provided to show equal protein loading.

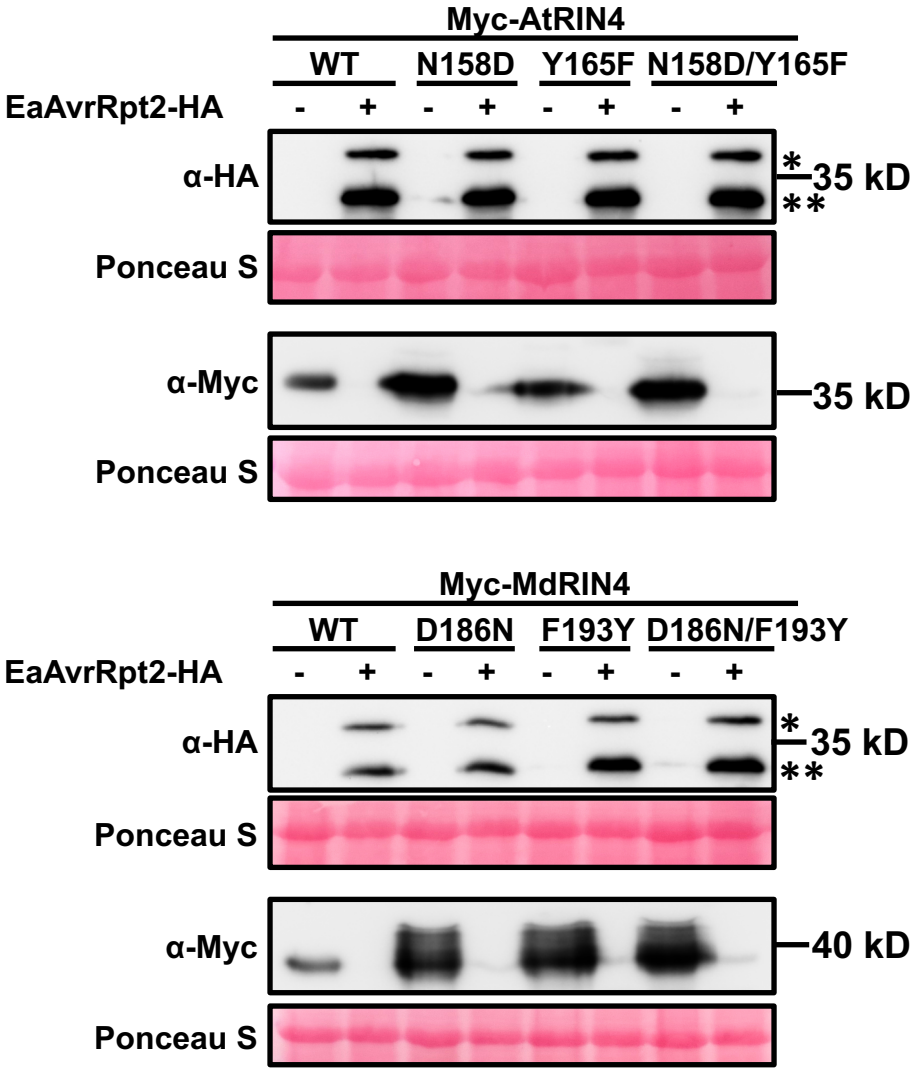

Fig. S9 The palmitoylation sequence motif is required for function of RIN4 full-length and ACP3 variants carrying reciprocal mutations at D/N or F/Y amino acid residues. (a) The full-length RIN4 variants with mutations in their palmitoylation sequence lose ability to suppress RPS2 auto-activity or activate MR5 upon EaAvrRpt2-directed cleavage. Agroinfiltration was carried out as described in Fig. S2. RIN4 AAA indicates RIN4 variants with mutations of three Cys to Ala residues in palmitoylation sequence. PCD symptoms were photographed at 3 dpi. Yellow asterisks indicate agroinfiltrated leaf area showing PCD. (b) Mutations in palmitoylation sequence lead to lower protein accumulation, possibly due loss of membrane localization. Agroinfiltration was carried out as mentioned in Fig. S8 and leaf samples were collected at 2 dpi and then protein extracts were probed with anti-Myc antibody. Ponceau staining the RuBisCO large subunit is provided to show equal protein loading. (c) RIN4 ACP3 variants with mutations in their palmitoylation sequence lose ability to activate MR5. Agroinfiltration was carried out as described in Fig. S2. ACP3 AAA indicates RIN4 ACP3 variants with mutations in palmitoylation sequence. PCD symptoms were photographed at 3 dpi. Yellow asterisks indicate agroinfiltrated leaf area showing PCD. (d) Mutations in palmitoylation sequence lead to changes of protein abundance. Agroinfiltration was carried out as mentioned in Fig. S8 and leaf samples were collected at 2 dpi and then protein extracts were probed with anti-Myc antibodies. Ponceau staining the RuBisCO large subunit is provided to show equal protein loading.

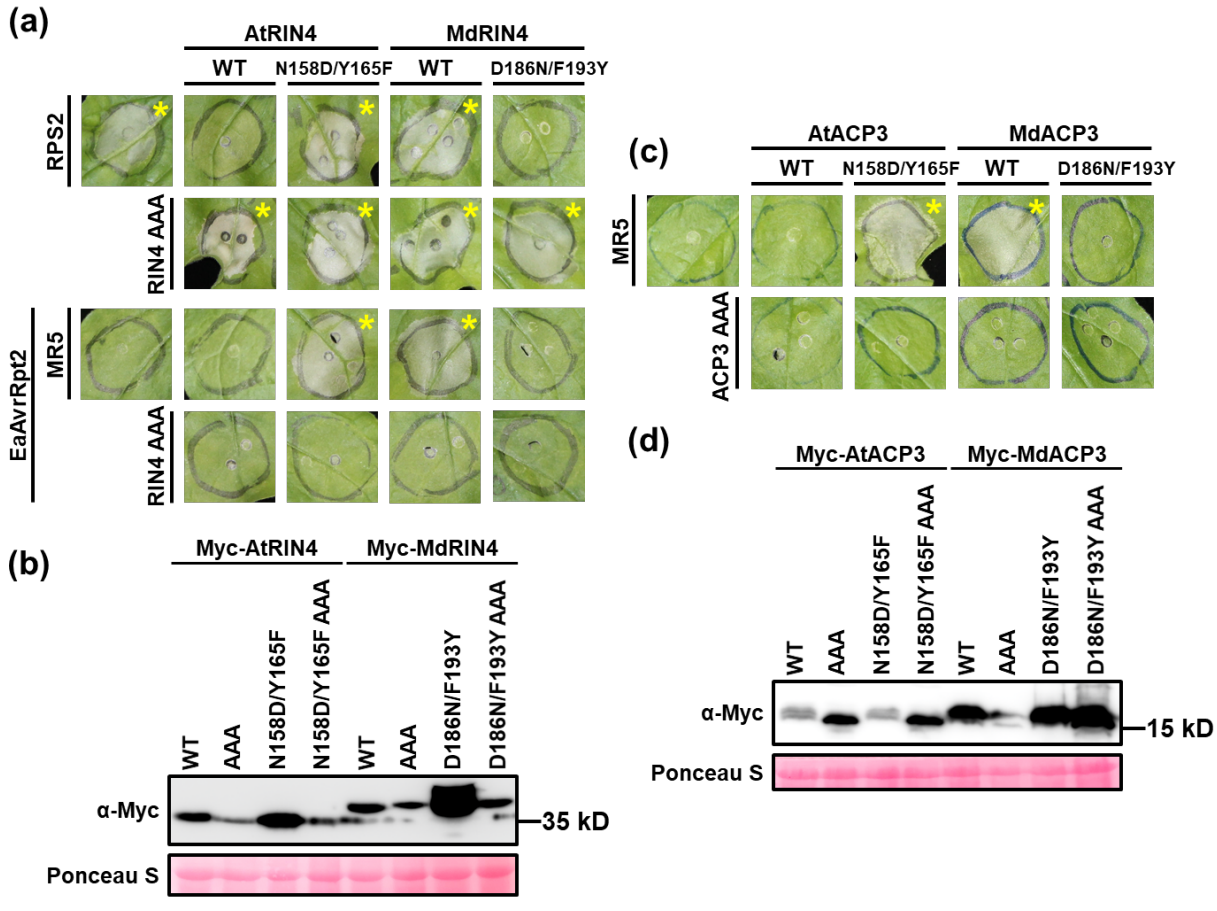

Fig. S10 MdRIN4$^{D186N/F193Y}$ ACP3 variant can suppress RPM1 and RPS2 mediated autoimmunity. (a) RPS2 or RPM1 (OD_{600}=0.05), RIN4 variants (OD_{600}=0.4) were co-expressed in *N. benthamiana* leaves by agroinfiltration and PCD symptoms were photographed at 2 dpi. (b) *N. benthamiana* leaves were agroinfiltrated as in (a). Graph represents electrolyte leakage levels measured in the infiltrated leaf samples. Statistical significance was assessed by one-way ANOVA test followed by Tukey-Kramer HSD analysis. Bars labeled with identical letter indicate that there is no significant statistical difference (*P*-value < 0.05). Each bar represents mean of 4 electrolyte leakage measurements. Error bars represent S.E.M. The experiment was conducted three times with similar results.

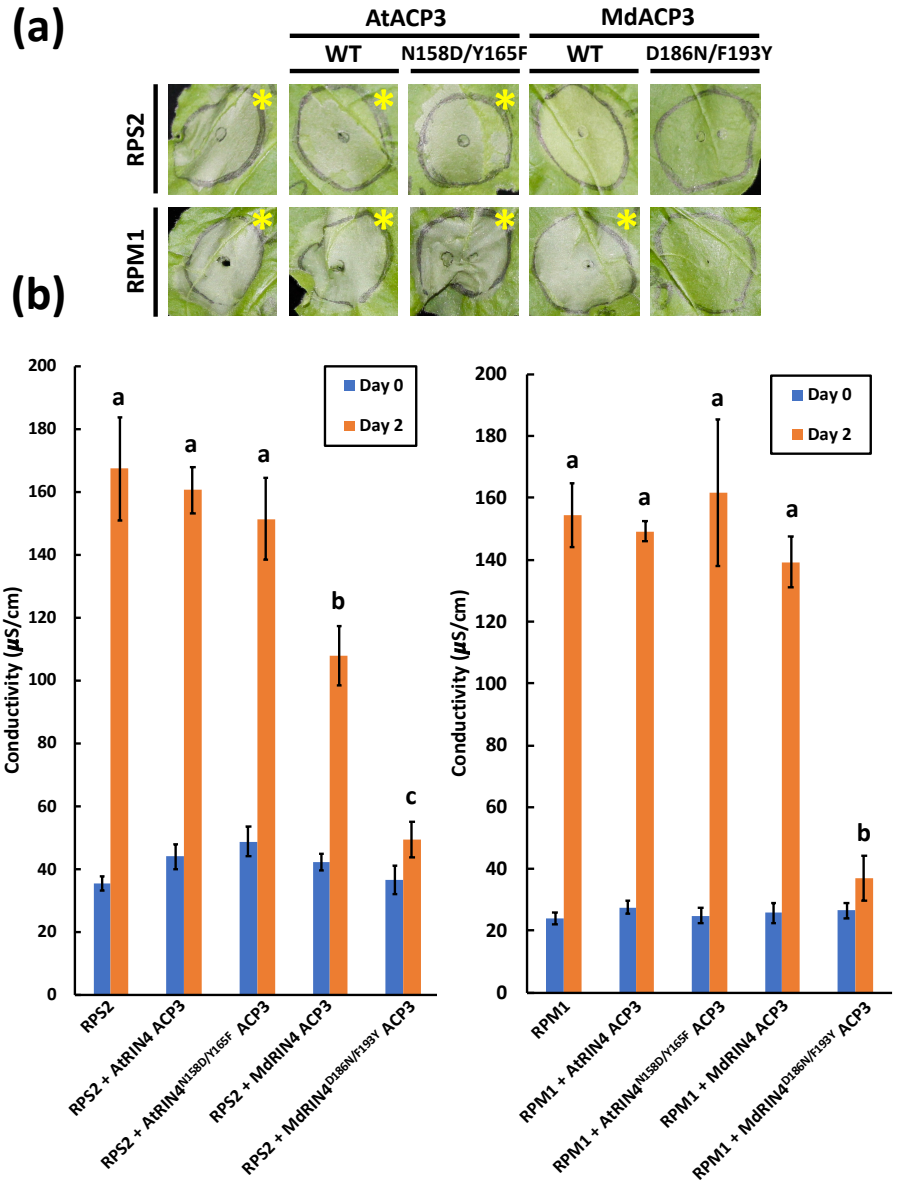

Fig. S11 RIN4 transgene expression in Arabidopsis transgenic lines. RIN4 transgene expression was assessed using semi-quantitative PCR approach. EF1α expression is used as a reference (27 cycles). RIN4 transcript was amplified with 33 cycles.

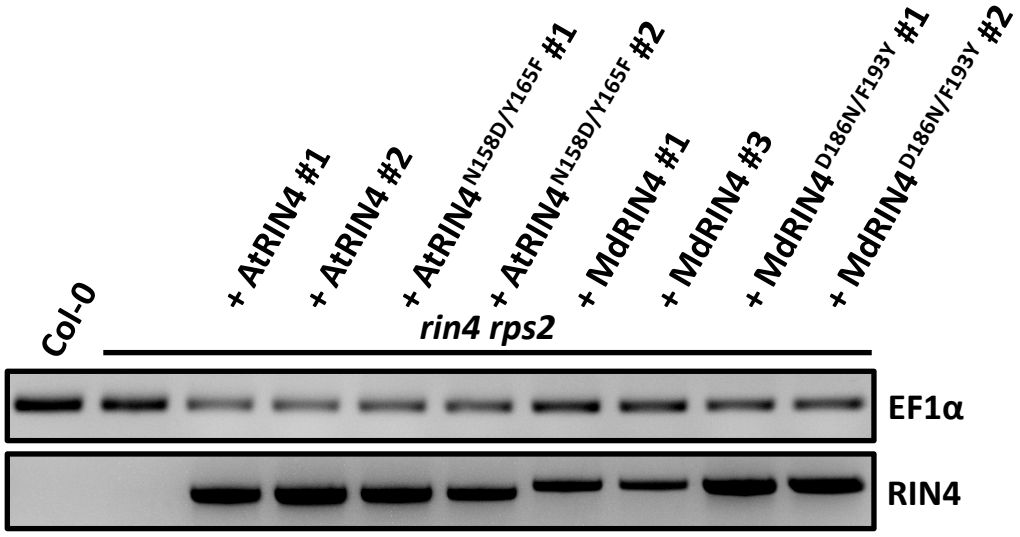

Table S1 Primers used in this study

	Primer name	**Primer sequence**
1	PsAvrRpt2_F	GGTCTCGAATGATGAAAATTGCTCCAGTTGCC
2	PsAvrRpt2_F	GGTCTCACGAAGCGGTAGAGCATTGCGTGT
3	EaAvrRpt2_F	GGTCTCGAATGAAAGTCAGTCATCTCACATCC
4	EaAvrRpt2_R	GGTCTCACGAAATTTTCACTGTATAACATGGCGTGT
5	RPS2_pt1_F	GGTCTCGAATGGATTTCATCTCATCTCTTATCGT
6	RPS2_pt1_R	GGTCTCACAACAACAAGAAACGTTTCTGTCT
7	RPS2_pt2_F	GGTCTCGGTTGCTAGATGATGTCTGGGAAG
8	RPS2_pt2_R	GGTCTCATTTCCAAGTATTCCAAGTCAGCG
9	RPS2_pt3_F	GGTCTCGGAAAACCTAACCACACTCGGTATC
10	RPS2_pt3_R	GGTCTCACGAAATTTGGAACAAAGCGCGGTAA
11	MR5_pt1_F	GGTCTCGAATGGGGGGAGAGGCTTTTCTT
12	MR5_pt1_R	GGTCTCAGACTCCACAGTTTGTTGTTCAAT
13	MR5_pt2_F	GGTCTCGAGTCTATCAAATGAGCACGACA
14	MR5_pt2_R	GGTCTCACTTGAATGGGACCATTCTAGCAC
15	MR5_pt3_F	GGTCTCGCAAGCGACACAAGAGAAACAGAA
16	MR5_pt3_R	GGTCTCATGTATTCTTCTGAGATTTTGGGGAA
17	MR5_pt1_F	GGTCTCGTACAGATAAGAGATTGCAGAAGTTTGA
18	MR5_pt1_F	GGTCTCACGAAAATCATCTTCCAATCTATATCTATGTA
19	RPM1_pt1_F	GGTCTCGAATGGCTTCGGCTACTGTTGATTT
20	RPM1_pt1_R	GGTCTCACTCTTTCTTTTCATCCGATAGTTCACA
21	RPM1_pt2_F	GGTCTCGAGAGGCTCATTAGGATGTGGATG
22	RPM1_pt2_R	GGTCTCACGAAAGATGAGAGGCTCACATAGAAAGAG
23	AtRIN4_F	GGTCTCGAATGGCACGTTCGAATGTACCA
24	AtRIN4_R	GGTCTCAAAGCTCATTTTCCTCCAAAGCCAAAGCA
25	MdRIN4_F	GGTCTCGAATGGCACAACGTTCACATGTAC

26	MdRIN4_R	GGTCTCACGAATCATTTTCTGCCCCATGGAAAG
27	MdRIN4_CLV1-2_R for Chimeric RIN4	GGTCTCAAAATTTGGGAACAGCAGCACCTTTC
28	AtRIN4_CLV3_F for Chimeric RIN4	GGTCTCGATTTGGTGACTGGGACGAGAACAAC
29	AtRIN4_CLV1-2_R for Chimeric RIN4	GGTCTCAGAATTTAGGCACCACTGTGAC
30	MdRIN4_CLV3_F for Chimeric RIN4	GGTCTCGATTCGGCGAGTGGGATGAGAAC
31	GFP_F	GGTCTCGAATGGTGAGCAAGGGCGAGGAG
32	AtRIN4_CLV1_R	GGTCTCACGAATCATCCAAATTTTGGTACATTCGAACG
33	MdRIN4_CLV1_R	GGTCTCACGAATCAGCCAAACTTTGGTACATGTGAAC
34	AtRIN4_CLV2_F	GGTCTCGAATGAACTGGGAAGCTGAGGAGAAT
35	AtRIN4_CLV2_R	GGTCTCACGAATCAACCGAATTTAGGCACCACTGT
36	MdRIN4_CLV2_F	GGTCTCGAATGAACTGGGAAGACCAAGAAAGTGT
37	MdRIN4_CLV2_R	GGTCTCACGAATCAGCCAAATTTGGGAACAGCAGC
38	AtRIN4_CLV3_F	GGTCTCGAATGGACTGGGACGAGAACAACCC
39	AtRIN4_CLV3_R	GGTCTCACGAATCATTTTCCTCCAAAGCCAAAGC
40	MdRIN4_CLV3_F	GGTCTCGAATGGAGTGGGATGAGAACGACCCG
41	MdRIN4_CLV3_R	GGTCTCACGAATCATTTTCTGCCCCATGGAAAG
42	AtRIN4_CLV3_pt1_R for Chimeric CLV3	GGTCTCAGCCTTCTCTTCACGGACTTTATTGAAGA
43	MdRIN4_CLV3_pt2_F for Chimeric CLV3	GGTCTCAAGGCGGGAAAAGCACCAGG
44	MdRIN4_CLV3_pt1_R for Chimeric CLV3	GGTCTCACTTCTCTCCTCCCGCACTTTGTTG
45	AtRIN4_CLV3_pt2_F for Chimeric CLV3	GGTCTCAGAAGTTCTGGAGCAAATGTGAGT

46	PbRIN4_F	GGTCTCAAATGGCACAACGTTCACATGTACCAAAGTTT
47	PbRIN4_R	GGTCTCAAAGCTCATTTTCTGCCCCACGGAA
48	EaAvrRpt2_C88A_F	CAACAGAATGAGCGAATGGGCGCCTGGTATGCCTGCACCAG
49	EaAvrRpt2_C88A_F	CTGGTGCAGGCATACCAGGCGCCCATTCGCTCATTCTGTTG
50	PsAvrRpt2_C122A_F	CGTATCCCAAGGTAATGAGCGAATGGGAGCTTGGTATGCCTGC
51	PsAvrRpt2_C122A_R	GCAGGCATACCAAGCTCCCATTCGCTCATTACCTTGGGATACG
52	MR5_K206A_F	GTATGGCTGGAGTCGGAGCGACAACACTTGCTGGAC
53	MR5_K206A_R	GTCCAGCAAGTGTTGTCGCTCCGACTCCAGCCATAC
54	MR5_D493V_F	TTTCAAAATATGTGATGCATGTCCTTATTGGTGATTTAGCACG
55	MR5_D493V_R	CGTGCTAAATCACCAATAAGGACATGCATCACATATTTTGAAA
56	MR5_D493N_F	CAAAATATGTGATGCATAACCTTATTGGTGATTTAGC
57	MR5_D493N_R	GCTAAATCACCAATAAGGTTATGCATCACATATTTTG
58	MdRIN4_F10A_F RCS1_mut	GTTCACATGTACCAAAGGCTGGCAATTGGGAAGACC
59	MdRIN4_F10A_R RCS1_mut	GGTCTTCCCAATTGCCAGCCTTTGGTACATGTGAAC
60	MdRIN4_F179A_F RCS2_mut	GGTGCTGCTGTTCCCAAAGCTGGCGAGTGGGATGAG
61	MdRIN4_F179A_R RCS2_mut	CTCATCCCACTCGCCAGCTTTGGGAACAGCAGCACC
62	MdRIN4_CCC_to_ACA_F GPI anchor mut	CAATGACAGTGCCAAGGCTTGCGCCTTTCCATGGGGC
63	MdRIN4_CCC_to_ACA_R GPI anchor mut	GCCCCATGGAAAGGCGCAAGCCTTGGCACTGTCATTG
64	MdRIN4_ACA_to_AAA_F GPI anchor mut	CAATGACAGTGCCAAGGCTGCCGCCTTTCCATGGGGC
65	MdRIN4_ACA_to_AAA_R GPI anchor mut	GCCCCATGGAAAGGCGGCAGCCTTGGCACTGTCATTG
66	AtRIN4_D153E_F	GGTCTCGAATGGAGTGGGACGAGAACAACCCGTC
67	AtRIN4_D153E_R	GACGGGTTGTTCTCGTCCCACTCCATTCGAGACC
68	AtRIN4_N158D_F	GGTGACTGGGACGAGAACGACCCGTCATCAGCTGA
69	AtRIN4_N158D_R	TCAGCTGATGACGGGTCGTTCTCGTCCCAGTCACC

70	AtRIN4_S160A_F	GGGACGAGAACAACCCGGCATCAGCTGACGGATAC
71	AtRIN4_S160A_R	GTATCCGTCAGCTGATGCCGGGTTGTTCTCGTCCC
72	AtRIN4_Y165F_F	CATCAGCTGACGGATTCACGCATATCTTCAATAA
73	AtRIN4_Y165F_R	TTATTGAAGATATGCGTGAATCCGTCAGCTGATG
74	MdtRIN4_E181D_F	GGTCTCGAATGGATTGGGATGAGAACGACCCGGC
75	MdRIN4_E181D_R	GCCGGGTCGTTCTCATCCCAATCCATTCGAGACC
76	MdRIN4_D186N_F	GGCGAGTGGGATGAGAACAACCCGGCATCAGCTG
77	MdRIN4_D186N_R	TCAGCTGATGCCGGGTTGTTCTCATCCCACTCGC
78	MdRIN4_A188S_F	GGGATGAGAACGACCCGTCATCAGCTGATGGTT
79	MdRIN4_A188S_R	AACCATCAGCTGATGACGGGTCGTTCTCATCCC
80	MdRIN4_F193Y_F	CATCAGCTGATGGTTACACTCATATATTCAACAA
81	MdRIN4_F193Y_R	TTGTTGAATATATGAGTGTAACCATCAGCTGATG

Table S2 Table of approximate molecular weights of protein products and their fragments used in this study

Protein name	Protein tag	Predicted size (kD)
PsAvrRpt2	C-terminal, 6xHA	36
PsAvrRpt2^{C122A}	C-terminal, 6xHA	36
EaAvrRpt2	C-terminal, 6xHA	32
EaAvrRpt2^{C88A}	C-terminal, 6xHA	32
AtRIN4	N-terminal, 4xMyc	28
MdRIN4-1	N-terminal, 4xMyc	31
MdRIN4-2	N-terminal, 4xMyc	32
MR5	C-terminal, 3xFLAG	161
MR5^{K206A}	C-terminal, 3xFLAG	161
MR5^{D493V}	C-terminal, 3xFLAG	161
MR5^{D493N}	C-terminal, 3xFLAG	161
MR5$^{K206A/D493V}$	C-terminal, 3xFLAG	161
RPS2	C-terminal, 3xFLAG	108
A1-2M3	N-terminal, 4xMyc	28
M1-2A3	N-terminal, 4xMyc	31
MdRIN4-1^{F10A}	N-terminal, 4xMyc	31
MdRIN4-1^{F179A}	N-terminal, 4xMyc	31
MdRIN4-1$^{F10A/F179A}$	N-terminal, 4xMyc	31
AtRIN4_ACP3	N-terminal, 4xMyc	11
MdRIN4-1_ACP3	N-terminal, 4xMyc	11
M-A_ACP3	N-terminal, 4xMyc	11
A-M_ACP3	N-terminal, 4xMyc	11
AtRIN4_ACP3^{N158D}	N-terminal, 4xMyc	11
AtRIN4_ACP3^{Y165F}	N-terminal, 4xMyc	11
AtRIN4_ACP3$^{N158D/Y165F}$	N-terminal, 4xMyc	11
MdRIN4-1_ACP3^{D186N}	N-terminal, 4xMyc	11
MdRIN4-1_ACP3^{F193Y}	N-terminal, 4xMyc	11
MdRIN4-1_ACP3$^{D186N/F193Y}$	N-terminal, 4xMyc	11
RPM1	C-terminal, GFP	134
AtRIN4	N-terminal, 3xFLAG	27
AtRIN4$^{N158D/Y165F}$	N-terminal, 3xFLAG	27
MdRIN4-1	N-terminal, 3xFLAG	30
MdRIN4-1$^{D186N/F193Y}$	N-terminal, 3xFLAG	30
RIPK	C-terminal, 3xHA	55
AtRIN4$^{N158D/Y165F}$	N-terminal, 4xMyc	28
MdRIN4-1$^{D186N/F193Y}$	N-terminal, 4xMyc	31
AvrRpm1	C-terminal, GFP	51

Methods S1 Quantitative RT-PCR

RNA was extracted from BASTA selected *Arabidopsis thaliana* T2 plants. RNA quality and quantity was measured and equalized prior to cDNA synthesis. EF1α transcript amplification was used as the reference. We used primers which amplify the whole RIN4 cDNA together with the protein tag region in order to detect transgene expression (for primers see Table S1).

Methods S2 RIN4 homolog and CNL phylogenetic analysis

Sequences of RIN4 homologs were downloaded from NCBI refseq database based on their similarity to *Arabidopsis thaliana* RIN4 protein sequence. We further used only the RIN4 homologs carrying two NOI-domains and two AvrRpt2 cleavage sites (consensus: [LVI]PxFGxW). In addition we excluded all the RIN4 homologs with disrupted or absent membrane anchoring domain in its C-terminus. The protein sequences showing more than 90% identity in the same species were discarded and the shortlisted RIN4 homologs were aligned using ClustalW. Neighbor-Joining phylogenetic tree was built using Geneious Prime tree builder with 100 bootstrap replicates. Only nodes with bootstrap support more than 70% were considered for final tree.

Protein sequences of reference CNLs were downloaded from Pathogen Receptor Genes database (http://www.prgdb.org). As comparison of the full length NLRs can lead to potentially false implication due to rapid rearrangement in LRR region, we only used truncated sequences containing the coiled-coil and NB-ARC regions based on InterProScan annotation. The resulted truncated protein sequences were aligned with ClustalW and a Neighbor-Joining phylogenetic tree was built using Geneious Prime tree builder with 100 bootstrap replicates. Only nodes with bootstrap support more than 70% were considered for final tree.